ChemComm

COMMUNICATION

View Article Online
View Journal | View Issue

Cite this: *Chem. Commun.*, 2025, **61**, 740

Received 14th October 2024,
Accepted 2nd December 2024

DOI: 10.1039/d4cc05419a

rsc.li/chemcomm

One-pot synthesis of supported sub-micron $LaNi_5$ for hydrogen storage in a carbazole-type liquid organic hydrogen carrier†

Hongen Yu, *[ab] Yuxuan Shi,[a] Zewei Xie,[b] Rumei Jin,[b] Youyu Lin,[b] Dongsheng Geng,[a] Xingguo Li[b] and Jie Zheng *[b]

Metal hydrides are promising catalysts in hydrogen-involving reactions. However, downsizing and loading metal hydrides is difficult due to their sensitivity towards oxygen and water. Here, a simple one-pot molten salt synthetical method is proposed to synthesize porous $La(OH)_3$-supported $LaNi_5$. The as-synthesized catalyst shows an evident improvement in catalyzing reversible hydrogen storage in liquid organic hydrogen carrier *N*-ethylcarbazole.

Metal hydrides (MHs) have long been utilized as efficient hydrogen storage materials due to their unique hydrogen absorption–desorption features.[1–4] The multiple H-bonding sites and surface H-species of MHs render them promising hydrogenation and dehydrogenation catalysts, especially in reactions such as olefin hydrogenation, CO_2 hydrogenation, NH_3 synthesis, and H_2 storage in liquid organic hydrogen carriers (LOHCs).[5,6] LOHCs are newly-emerging liquid-state hydrogen storage materials that utilize the hydrogenation and dehydrogenation of aromatic and N-heterocycle rings to store H_2, which is considered a possible solution to large-scale, long-distance H_2 transportation.[7,8] The hydrogenation and dehydrogenation of LOHCs generally occur under 200 °C with no oxygen-containing species involved, making them an appropriate model system to investigate MH-type catalysts. Moreover, studying MH-type catalysts for LOHC is beneficial for developing MH/LOHC hybrid H_2 storage systems adaptable to diverse application scenarios in the future.

Based on this concept, Chen *et al.* investigated $LaNi_5$, $MlNi_5$, and Mg–Ni alloy as catalysts for the hydrogenation of benzene and toluene.[9–11] An *et al.* utilized NH_4F-treated $LaNi_5$ as a hydrogenation catalyst for *N*-ethylcarbazole (NEC).[12] Recently, our group has developed a series of YH_3-based materials for reversible H_2 storage in NEC.[13–16] Some of the MH-based catalysts show interesting dual functional catalytical activity in both the hydrogenation of NEC and the dehydrogenation of its hydrogen-rich counterpart 12H-NEC due to the fluctuating H-content in the solid solution region of MH catalysts.[15,16] Nevertheless, current MH-type catalysts suffer from two intrinsic drawbacks: (1) MH alone usually exhibits low or negligible catalytic activity and requires coupling with transition metals (TM). (2) Most MHs are sensitive to O_2 and H_2O, which hinders their activity and stability enhancement owing to limited downsizing and loading methods. The coupling methods of MH and TM are often confined to mechanical approaches like simple mixing and ball milling, making it difficult to precisely construct the interface.

We have partially solved these problems by bottom-up synthesis of sub-μm TM-containing $LaNi_5$-based catalysts.[17–19] However, considering the high reducing temperature (600–800 °C) and strong-reductive environment (CaH_2 as reducing reagent) during the synthetical process, further activity enhancements *via* dispersing sub-μm $LaNi_5$ on supports with a large surface area is demanding. Conventional loading methods like incipient wetness, sol–gel, and ion exchange[20] are not suitable for synthesizing supported-$LaNi_5$, as common oxide support Al_2O_3, TiO_2 will be simultaneously reduced, forming other unintended byproducts like Ni–Al and Ni–Ti alloys during the synthetical process. Although there are several reports on the synthesis of supported MgH_2 nanoparticles that utilize the decomposition of organometallic precursors,[21–23] it is hard to apply it to $LaNi_5$ alloy due to the highly negative reduction potential of La^{3+}/La^{2+} (−2.38 eV) and the lack of corresponding organic compounds with the exact composition.

Here in the current paper, we propose a novel one-pot method to synthesize sub-μm $LaNi_5$ supported on porous metal hydroxide $La(OH)_3$. Under the catalysis of the as-synthesized $LaNi_5/La(OH)_3$, NEC exhibits a hydrogenation rate of 0.028 mol h^{-1} g^{-1} (180 °C, 7 MPa H_2) and dehydrogenation

[a] *Jiangsu Key Laboratory of New Energy Devices & Interface Science, School of Chemistry and Materials Science, Nanjing University of Information Science & Technology (NUIST), Nanjing 210000, China. E-mail: yuhongen@nuist.edu.cn*

[b] *Beijing National Laboratory for Molecular Sciences (BNLMS), College of Chemistry and Molecular Engineering, Peking University, Beijing 100871, China. E-mail: zhengjie@pku.edu.cn*

† Electronic supplementary information (ESI) available. See DOI: https://doi.org/10.1039/d4cc05419a

rate of 0.019 mol h^{-1} g^{-1} (200 °C, 0.1 MPa H_2), with a final H_2 uptake and release amount of 5.75 wt%. Loading of sub-μm $LaNi_5$ on $La(OH)_3$ significantly increases its catalytic activity and selectivity towards fully hydrogenated and dehydrogenated products as a result of the synergetic effect between $LaNi_5$ and $La(OH)_3$, together with the etching of supports by molten salt to create porous $La(OH)_3$ with a relatively large surface area.

$LaNi_5/La(OH)_3$ is synthesized *via* a one-pot high-temperature molten salt reduction method with excessive La in the precursor. In a typical experiment, 12.0 mmol $La(NO_3)_3{\cdot}6H_2O$ and 5.00 mmol $Ni(NO_3)_2{\cdot}6H_2O$ were dissolved in 15.0 mL deionized water (20 wt% $LaNi_5$ loading amount), then Ni^{2+} and La^{3+} ions were co-precipitated by 3.33 mol L^{-1} NaOH aqueous solution, the precipitates were dried at 60 °C overnight and calcined at 600 °C for 3 hours to convert into a black La–Ni–O precursor powder. 1.20 g of precursor was mixed with 2.00 g KCl and 0.40 g CaH_2, then heated at 700 °C for 2 h under Ar protection (flow rate 70 sccm). The calcined mixture was washed with 0.100 mol L^{-1} acetic acid under Ar protection, and the final products were obtained after centrifugation, washing, and vacuum drying.

The ratio of precursor, molten salt, and reducing agent is vital in synthesizing $LaNi_5/La(OH)_3$. As shown in Fig. 1a, when the input of CaH_2 is only 0.05 g, no reducing products are observed, as the CaH_2 input increases to 0.25 g, Ni is generated, further increasing the CaH_2 input to 0.40 g, La-precursor is reduced and alloyed with existing Ni to form $LaNi_5$ alloy with some of the Ni phase preserved. A byproduct that cannot be ignored is LaOCl, which has a matlockite-type tetragonal structure of alternating $(LaO)_n^{n+}$ cation and Cl^- anion layers aligning along the crystallographic *c* direction.[24,25] In the comparative experiment, catalysts with a high LaOCl content demonstrate poor catalytic activity, especially in 12H-NEC dehydrogenation (Fig. S1, ESI†). To minimize the generation of LaOCl, the input of KCl is adjusted, according to XRD in Fig. 1b, too much or too little KCl can lead to significant formation of LaOCl, and the optimized KCl input is 2.00 g. The formation of LaOCl is inevitable as in the Cl^--rich environment, the following reaction reaches the equilibrium:

$$La_2O_3 + 2Cl^- \rightarrow 2LaOCl + O^{2-} \quad (1)$$

In reaction (1), the generated LaOCl dissolved in molten salt KCl. KCl serves both as a reactant and solvent. Decreasing solvent KCl leads to the precipitation of LaOCl, and increasing reactant KCl leads to an increase of Cl^- concentration, both shifting the equilibrium in reaction (1) towards LaOCl formation. Under the optimized feeding ratio of 1.2 : 2.0 : 0.4 (precursor : KCl : CaH_2), the product shows the lowest amount of about 3% LaOCl by semi-quantitative XRD analysis.

As demonstrated in Fig. 2a, the obtained $LaNi_5$ alloy exhibits particle sizes at the magnitude of tens nanometers with a short column morphology, which is slightly smaller than unsupported sub-μm $LaNi_5$[17] due to the dispersive effect of excessive $La(OH)_3$. HRTEM shown in Fig. 2c and d confirms the core–shell structure of sub-μm $LaNi_5$. The resolved interplanar spacings of 0.318 nm and 0.264 nm outside sub-μm $LaNi_5$ are designated to the (011) and (012) planes of $La(OH)_3$ and LaOCl, respectively (Fig. 2e). Fig. 2b depicts the deconvoluted XPS results of the as-synthesized catalysts, and the spectrum is complicated due to the overlap of the La $3d_{3/2}$ and Ni $2p_{3/2}$ orbitals. The La $3d_{5/2}$ peaks at 834.3 eV and 837.8 eV represent La(III) and its satellite peaks, and the binding energy difference between the two peaks is 3.5 eV, indicating that surface La mainly exists as $La(OH)_3$.[26,27] The intensity of Ni $2p_{1/2}$ is too feeble to resolve the exact forms of Ni on the surface.

The comparison sample Ni/La_2O_3 (Ni loading 20 wt%) was synthesized by the same co-precipitation-reduction method. The Ni/La_2O_3 catalyst was reduced directly from La–Ni–O precursor with H_2/Ar (20 sccm: 50 sccm) in a tube furnace. XRD and SEM of the La–Ni–O precursor (Fig. 3b and c) confirms that it consists of $La(OH)_3$ and La_3NiO_8 with an aggregated ball-like

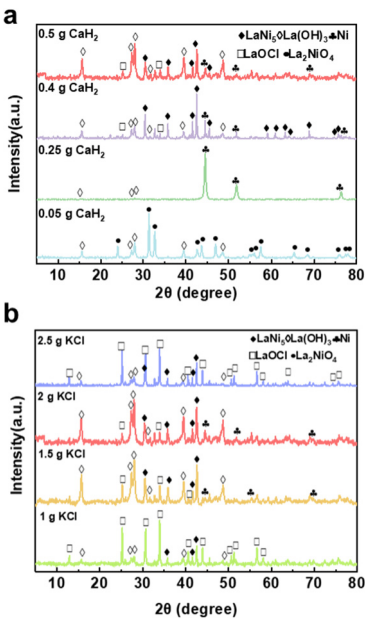

Fig. 1 XRD of the reduction products of 1.20 g La–Ni–O precursor (La : Ni = 12 : 5) in (a) 2.00 g KCl with varying amounts of CaH_2, and (b) 0.50 g CaH_2 with varying amounts of KCl.

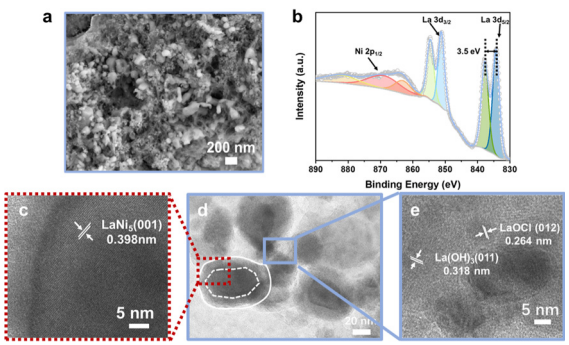

Fig. 2 (a) SEM, (b) deconvoluted XPS results of Ni 2p and La 3d orbital, and (c)–(e) HRTEM of the as-synthesized $LaNi_5/La(OH)_3$ (the core–shell-structure is highlighted).

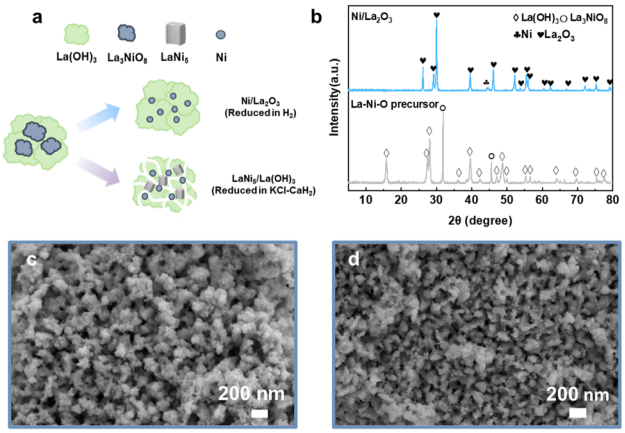

Fig. 3 (a) Schematic structure and (b) XRD of the La–Ni–O precursor and Ni/La_2O_3. SEM of (c) the La–Ni–O precursor and (d) Ni/La_2O_3.

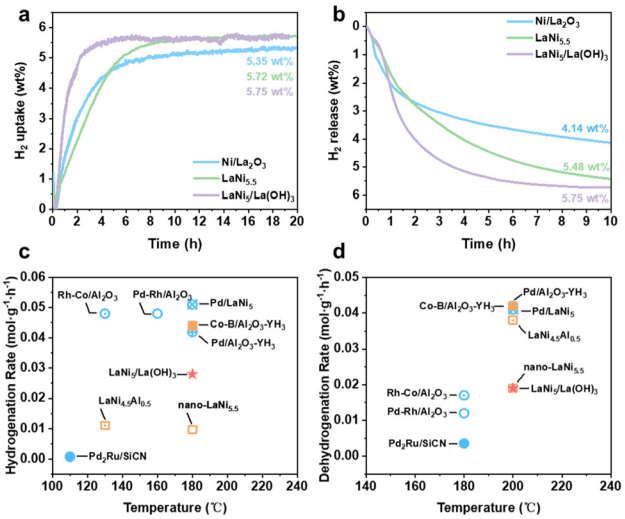

Fig. 4 (a) Hydrogen uptake and (b) release kinetics of NEC/12H-NEC catalyzed by Ni/La_2O_3, unsupported sub-μm $LaNi_{5.5}$, and $LaNi_5/La(OH)_3$. Hydrogenation and dehydrogenation reactions are carried out at 180 °C, 7 MPa H_2, and 200 °C, 0.1 MPa H_2, respectively, and the catalyst loading is 10 wt%. (c) and (d) Hydrogenation and dehydrogenation performances of this work compared with dual-functional catalysts for reversible H_2 storage of NEC reported in the literature.

morphology. Reduction in H_2/Ar doesn't change the overall morphology, which consists of Ni particles with a diameter of several nanometers attached on the surface of the $La(OH)_3$ support (Fig. 3b and d). On the other hand, reduction by KCl and CaH_2 breaks down the aggregated $La(OH)_3$ into smaller particles (Fig. 2a). The etching effect of molten-mixture KCl–CaH_2 is more prominent by comparing the surface area of the as-synthesized catalysts, as it increases from 11.4 $m^2\ g^{-1}$ for Ni/La_2O_3 to 93.9 $m^2\ g^{-1}$ for $LaNi_5/La(OH)_3$ (Fig. S2, ESI†). La and Ni disperse evenly on the supports in both catalysts as shown in EDS mapping (Fig. S3 and S4, ESI†). The schematic structures of the precursor and the two catalysts are illustrated in Fig. 3a.

The catalytical performances of Ni/La_2O_3, sub-μm $LaNi_{5.5}$, and $LaNi_5/La(OH)_3$ for NEC hydrogenation and 12H-NEC dehydrogenation are summarized in Fig. 4a and b. The reaction rate is calculated based on the converted amount of substances (1 mol) in unit time (1 h) on the unit mass of the catalyst (1 g). As we use consumed and produced H_2 to draw hydrogenation and dehydrogenation kinetics, the accurate consumption of reactants isn't recorded; here, the multi-step reaction is simplified to a single-step one. The conversion of the reactant is calculated based on H_2 consumption/production, taking the NEC hydrogenation reaction as an example:

$$r\ (\mathrm{mol\ h^{-1}\ g^{-1}}) = \frac{\frac{m_{\mathrm{NEC}}}{M_{\mathrm{NEC}}} \times \frac{x_1}{x_2}}{t_1 \times m_{\mathrm{catalyst}}} \qquad (2)$$

m_{NEC} represents the mass of the reactant, M_{NEC} represents the relative molecular mass of NEC, x_1 represents the actual H_2 uptake amount (wt%) in the first hour of reaction, x_2 represents theoretical capacity 5.8 wt%, t_1 is 1 h, and m_{catalyst} is the mass of the catalyst.

In NEC hydrogenation, $LaNi_5/La(OH)_3$ displays the highest catalytical activity of 0.028 mol h^{-1} g^{-1}, compared to 0.0096 mol h^{-1} g^{-1} of the unsupported sub-μm $LaNi_{5.5}$ and 0.015 mol h^{-1} g^{-1} of Ni/La_2O_3. In 12H-NEC dehydrogenation, $LaNi_5/La(OH)_3$ shows the highest catalytical activity of 0.019 mol h^{-1} g^{-1}, which equals that of unsupported sub-μm $LaNi_{5.5}$ and is higher than that of Ni/La_2O_3. $LaNi_5/La(OH)_3$ also demonstrates the highest selectivity towards the fully hydrogenated/dehydrogenated product; the 12H-NEC selectivity in NEC hydrogenation is 96.5%, and the NEC selectivity in 12H-NEC dehydrogenation is 100%, yielding 5.75 wt% reversible H_2 storage capacity in total. The NEC hydrogenation and 12H-NEC dehydrogenation rate in this work and those of other dual-functional catalysts reported in the literature[15–19,28–30] are compared in Fig. 4c and d.

$LaNi_5/La(OH)_3$ realizes superior NEC hydrogenation and equivalent 12H-NEC dehydrogenation catalytical performances compared to unsupported sub-μm $LaNi_{5.5}$, proving the advantages of dispersing the catalysts on $La(OH)_3$ supports. As alkaline oxides, La_2O_3 and $La(OH)_3$ are not ideal supports for NEC (de)hydrogenation,[31] but the loading process reduces the alloy particle size and increases the surface area, which is especially beneficial for enhancing catalytical activity in NEC hydrogenation. In the literature, Ni-based catalysts with large surface areas demonstrate considerable NEC hydrogenation activity but seldom serve as efficient 12H-NEC dehydrogenation catalysts.[32] The same phenomenon is observed in the current work, as under the catalysis of Ni/La_2O_3, only 4.14 wt% and H_2 are released after reacting for 10 hours. The outstanding catalytic dehydrogenation performance of $LaNi_5/La(OH)_3$ comes from $LaNi_5$ alloy. Under the dehydrogenation conditions (200 °C, 0.1 MPa H_2), the abundant H-bonding sites in the $LaNi_5$ lattice offer a low-energy-barrier H-transfer pathway to facilitate the dehydrogenation reaction.[19] The equilibrium metal-to-hydride transition pressure calculated by the CALPHAD method of $LaNi_5$ at 180 °C and 200 °C is 10.3 MPa and 14.7 MPa, which means that $LaNi_5$ utilizes the hydrogen-lean solid solution region in both NEC hydrogenation and 12H-NEC

dehydrogenation, explaining the more evident improvement of $LaNi_5/La(OH)_3$ in 12H-NEC dehydrogenation compared to La_2O_3-supported Ni-based catalysts. However, the cycling stability of $LaNi_5/La(OH)_3$ is unsatisfactory, and the $LaNi_5$ alloy phase completely decomposes into Ni after one H_2 storage cycle (Fig. S5, ESI†). Due to the intensified H_2-induced amorphization, weak metal-support interaction, and unstable metal-support interface, $LaNi_5/La(OH)_3$ is even more unstable than unsupported sub-μm $LaNi_{5.5}$.[17] It is necessary to further investigate support surface modification and post-synthetical methods to increase its thermal stability in the future.

In conclusion, supported-MH catalyst $LaNi_5/La(OH)_3$ is synthesized *via* a one-pot high-temperature molten salt reduction method with excessive La in the precursor. The etching effect of the molten mixture and the heat generated during $LaNi_5$ alloy formation greatly increased the surface area of $La(OH)_3$. The existence of the $La(OH)_3$ support helps decrease the particle size of $LaNi_5$ alloy at the magnitude of tens of nanometers. The NEC hydrogenation rate is boosted from 0.0096 mol h^{-1} g^{-1} of unsupported sub-μm $LaNi_{5.5}$ to 0.028 mol h^{-1} g^{-1} of $LaNi_5/La(OH)_3$, and the 12H-NEC dehydrogenation rate remains at 0.019 mol h^{-1} g^{-1}. $La(OH)_3$ with an elevated surface area is an appropriate support of Ni-based catalysts for reversible H_2 storage in NEC. The one-pot molten salt reduction method is a direct and effective way of synthesizing supported-MH catalysts, which is beneficial for future industrial applications.

This work was supported by NSFC (No. 22409094 and No. 22179002), the startup foundation for introducing talent of NUIST, MOST of China (No. 2021YFB4000603 and 2021 YFB4000601), and the PetroChina-Peking University strategic joint fundamental research project.

Data availability

The data supporting this article have been included in the paper.

Conflicts of interest

The authors declare no conflicts of interest.

References

1 J. Yang, A. Sudik, C. Wolverton and D. J. Siegel, *Chem. Soc. Rev.*, 2010, **39**, 656–675.
2 L. Schlapbach and A. Zuttel, *Nature*, 2001, **414**, 353–358.
3 Y. Liu, H. Pan, M. Gao and Q. Wang, *J. Mater. Chem.*, 2011, **21**, 4743–4755.
4 H. Pan, Y. Liu, M. Gao, Y. Zhu, Y. Lei and Q. Wang, *J. Alloys Compd.*, 2003, **351**, 228–234.
5 H. Yu, X. Li and J. Zheng, *ACS Catal.*, 2024, 3139–3157.
6 Q. Wang, Y. Guan, J. Guo and P. Chen, *Cell Rep. Phys. Sci.*, 2022, **3**, 1–29.
7 M. D. Allendorf, V. Stavila, J. L. Snider, M. Witman, M. E. Bowden, K. Brooks, B. L. Tran and T. Autrey, *Nat. Chem.*, 2022, **14**, 1214–1223.
8 D. Wei, X. Shi, R. Qu, K. Junge, H. Junge and M. Beller, *ACS Energy Lett.*, 2022, **7**, 3734–3752.
9 Y. An, C. P. Chen, G. H. Xu, G. M. Cai and Q. D. Wang, *J. Rare Earths*, 2002, **20**, 113–115.
10 Y. An, C. P. Chen, G. H. Xu, G. M. Cai and Q. D. Wang, *J. Rare Earths*, 2002, **20**, 231–233.
11 C. P. Chen, G. M. Cai, Y. Chen, Y. An, G. H. Xu and Q. D. Wang, *J. Alloys Compd.*, 2003, **350**, 275–279.
12 F. Wu, Y. An, L. Song, G. Xu and L. Xia, *Chem. React. Eng. Technol.*, 2015, **31**, 407–411.
13 Y. Wu, H. Yu, Y. Guo, X. Jiang, Y. Qi, B. Sun, H. Li, J. Zheng and X. Li, *Chem. Sci.*, 2019, **10**, 10459–10465.
14 Y. Wu, H. G. Yu, Y. R. Guo, Y. X. Zhang, X. J. Jiang, B. X. Sun, K. Fu, J. Chen, Y. Qi, J. Zheng and X. G. Li, *J. Mater. Chem. A*, 2019, **7**, 16677–16684.
15 Y. Wu, Y. Guo, H. Yu, X. Jiang, Y. Zhang, Y. Qi, K. Fu, L. Xie, G. Li, J. Zheng and X. Li, *CCS Chem.*, 2020, **2**, 974–984.
16 X. Yang, Y. Wu, H. Yu, M. Sun, J. Zheng, X. Li, W. Lin and Y. Wu, *Int. J. Hydrogen Energy*, 2020, **45**, 33657–33662.
17 H. Yu, X. Yang, X. Jiang, Y. Wu, S. Chen, W. Lin, Y. Wu, L. Xie, X. Li and J. Zheng, *Nano Energy*, 2021, **80**, 105476.
18 H. E. Yu, Y. Wu, S. P. Chen, Z. W. Xie, Y. M. Wu, N. Cheng, X. Yang, W. Lin, L. Xie, X. G. Li and J. Zheng, *Appl. Catal., B*, 2022, **317**, 121720.
19 H. Yu, Z. Zhang, X. Jin, X. Zhang, R. Jin, Y. Lin, Z. Xie, Y. Huang, T. Liu, X. Li, Q. Sun and J. Zheng, *ACS Catal.*, 2024, 10519–10528.
20 B. A. T. Mehrabadi, S. Eskandari, U. Khan, R. D. White and J. R. Regalbuto, *Advances in Catalysis*, ed. C. Song, Academic Press, 2017, vol. 61, pp. 1–35.
21 G. L. Xia, Y. B. Tan, X. W. Chen, D. L. Sun, Z. P. Guo, H. K. Liu, L. Z. Ouyang, M. Zhu and X. B. Yu, *Adv. Mater.*, 2015, **27**, 5981–5988.
22 K. J. Jeon, H. R. Moon, A. M. Ruminski, B. Jiang, C. Kisielowski, R. Bardhan and J. J. Urban, *Nat. Mater.*, 2011, **10**, 286.
23 X. Zhang, Y. Liu, Z. Ren, X. Zhang, J. Hu, Z. Huang, Y. Lu, M. Gao and H. Pan, *Energy Environ. Sci.*, 2021, **14**, 2302–2313.
24 G. Li, Z. Hou, C. Peng, W. Wang, Z. Cheng, C. Li, H. Lian and J. Lin, *Adv. Funct. Mater.*, 2010, **20**, 3446–3456.
25 Z. Xue, Y. Shen, P. Li, Y. Zhang, J. Li, B. Qin, J. Zhang, Y. Zeng and S. Zhu, *Small*, 2018, **14**, 1800927.
26 J. P. H. Li, X. Zhou, Y. Pang, L. Zhu, E. I. Vovk, L. Cong, A. P. Van Bavel, S. Li and Y. Yang, *Phys. Chem. Chem. Phys.*, 2019, **21**, 22351–22358.
27 M. F. Sunding, K. Hadidi, S. Diplas, O. M. Løvvik, T. E. Norby and A. E. Gunnæs, *J. Electron Spectrosc. Relat. Phenom.*, 2011, **184**, 399–409.
28 D. Forberg, T. Schwob, M. Zaheer, M. Friedrich, N. Miyajima and R. Kempe, *Nat. Commun.*, 2016, **7**, 13201.
29 W. J. Xue, H. X. Liu, B. H. Mao, H. L. Liu, M. H. Qiu, C. G. Yang, X. Q. Chen and Y. H. Sun, *Chem. Eng. J.*, 2021, **421**, 127781.
30 W. Xue, H. Liu, B. Zhao, L. Ge, S. Yang, M. Qiu, J. Li, W. Han and X. Chen, *Appl. Catal., B*, 2023, **327**, 122453.
31 K. M. Eblagon, D. Rentsch, O. Friedrichs, A. Remhof, A. Zuettel, A. J. Ramirez-Cuesta and S. C. Tsang, *Int. J. Hydrogen Energy*, 2010, **35**, 11609–11621.
32 X. Ye, Y. An and G. Xu, *J. Alloys Compd.*, 2011, **509**, 152–156.